THE JOURNAL OF PHYSICAL CHEMISTRY A

ARTICLE

pubs.acs.org/JPCA

XUV Free-Electron Laser Desorption of NO from Graphite (0001)

Björn Siemer,[*,†] Tim Hoger,[†] Marco Rutkowski,[†] Stefan Düsterer,[‡] and Helmut Zacharias[†]

[†]Physikalisches Institut, Westfälische Wilhelms-Universität Münster, Wilhelm Klemm Strasse 10, 48149 Münster, Germany

[‡]Deutsches Elektronen Synchrotron DESY, HASYLAB, Notkestrasse 85, 22603 Hamburg, Germany

ABSTRACT: We report results of femtosecond laser induced desorption of NO from highly oriented pyrolytic graphite using XUV photon energies of $h\nu$ = 38 eV and $h\nu$ = 57 eV. Femtosecond pulses with a pulse energy of up to 40 μJ and about 30 fs duration generated at FLASH are applied. The desorbed molecules are detected with rovibrational state selectivity by (1 + 1) REMPI in the $A^2\Sigma^+ \leftarrow X^2\Pi$ γ-bands around λ = 226 nm. A nonlinear desorption yield of neutral NO is observed with an exponent of $m = 1.4 \pm 0.2$. At a fluence of about 4 mJ/cm^2 a desorption cross section of $\sigma_1 = (1.1 \pm 0.4) \times 10^{-17}$ cm^2 is observed, accompanied with a lower one of $\sigma_2 = (2.6 \pm 0.3) \times 10^{-19}$ cm^2 observable at higher total fluence. A nonthermal rovibrational population distribution is observed with an average rotational energy of $\langle E_{rot} \rangle$ = 38.6 meV (311 cm^{-1}), a vibrational energy of $\langle E_{vib} \rangle$ = 136 meV (1097 cm^{-1}) and an electronic energy of $\langle E_{el} \rangle$ = 3.9 meV (31 cm^{-1}).

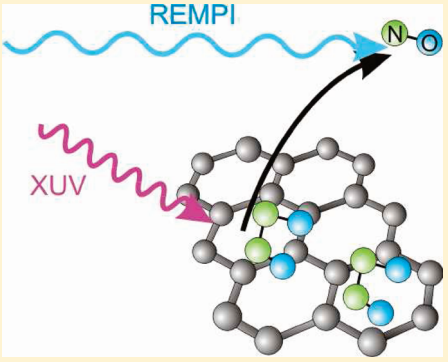

INTRODUCTION

The understanding of photoreactions on surfaces has considerably advanced in the last decades. On metal surfaces the primarily excited hot electrons can interact directly with adsorbate molecules. At high photon intensities, as provided by femtosecond optical pulses, a very hot and nonthermal electron gas is created on a femtosecond time scale via inelastic electron−electron interactions. Electrons in this highly exited state may then subsequently interact with adsorbed molecules.[1] On insulating surfaces with an electronic band gap like oxides, direct charge transfer excitations[2−4] of the substrate−adsorbate complex often constitute the dominating primary excitation step.[5] In the past, femtosecond pulses for laser desorption have been employed mainly in the visible and near-UV spectral range ($h\nu \lesssim$ 4.6 eV). Photon energies extending to $h\nu \lesssim$ 6.4 eV[6] and occasionally even to $h\nu \sim$ 7.9 eV (157 nm)[7] were accessible only with nanosecond pulses due to the available excimer laser sources. On the other hand, synchrotrons readily provide photons with energies in the extreme UV (XUV) and soft X-ray spectral range, albeit at very low photon fluxes for the individual light pulses.

At high photon energies, direct adsorbate electronic excitation has led to the development of the very successful Menzel-Gomer-Redhead (MGR) model of photon-induced desorption.[8,9] This photoreaction scheme leads in the primary step to electronically highly excited species, followed by ionization or dissociation reactions or both. It is therefore expected that products in an ionized state or with high kinetic energies leave the surface.

Despite the large absorption cross section of such direct processes in the XUV, most impinging photons are nevertheless not absorbed in a single monolayer of an adsorbate. Instead, the vast majority of incident photons are absorbed only in thick adsorbate layers or by the substrate. When photoreactions are initiated in various depths of a thick adsorbate layer, collision cascades will have a significant influence on the kinetic energy distribution of the products formed[10] and possibly also on the distribution and chemical nature of the constituents. On the other hand, primary excitation of substrate electrons is followed on a 10−100 femtosecond time scale by a rapid decrease of their average energy due to electron−electron collisions, accompanied by an exponential growth of their number density. Therefore, the excitation of an adsorbate−substrate system with XUV photons initiates various competing photoreaction processes, which do not occur at low photon energies. The identification of major reaction channels is of central interest at these photon energies.

The investigation of photochemical surface processes at such high photon energies is further important for an understanding of molecule formation on interstellar grains. Besides the most abundant hydrogen molecule, also, carbon, nitrogen, and oxygen containing molecules are formed at such grains.[11] Due to its high mobility, the formation of molecular hydrogen occurs thermally via surface reactions, even at very low temperatures and, therefore, even in dense, dark molecular clouds.[12,13] The formation of new bonds between the heavier atoms requires thermally very long times or may be stimulated by photons. In particular in the vicinity of new-born stars high fluxes of high-energy photons penetrate into such clouds, and may open new reaction pathways with unexpected products. The grains are mainly of carbonaceous or silicate type, with a weak interaction with adsorbates. These substrates on the other hand show a large bandgap, thus requiring high photon energies when reactions shall be initiated via the substrate.

Special Issue: J. Peter Toennies Festschrift

Received: February 4, 2011
Revised: May 5, 2011
Published: May 18, 2011

The appearance of free-electron lasers (FEL) that operate in the XUV and soft X-ray regime providing femtosecond pulse durations and high pulse energies[14] make detailed studies of dynamic processes in this spectral regime feasible.[15,16] As a first step, highly oriented pyrolytic graphite (HOPG) seems to be an adequate model system to study such processes due to its weak interaction with many adsorbates. In graphite, the density-of-states near the Fermi energy E_F is low. Further, in the visible and UV spectral range, optical excitations are only possible in the vicinity of the K point of the Brillouin zone, the photons then interact with electrons of high momentum.[17] Employing XUV photons allows access to electrons in the whole Brillouin zone, making further use of high densities of initial and final states. Therefore, questions regarding the general electron dynamics initiated by high energy photons in adsorbate−surface systems as well as a possible direct excitation in the adsorbate alone may be addressed. In this contribution we report results on nitric oxide desorption from $(NO)_2$/graphite induced at two different photon energies in the XUV using the radiation provided by the free-electron laser in Hamburg (FLASH).

EXPERIMENTAL SECTION

A highly oriented pyrolytic graphite (HOPG) sample with a mosaic angle of 0.4° is mounted on a coldfinger in an ultrahigh vacuum (UHV) chamber. For preparation, the HOPG is cleaved with adhesive tape and annealed under vacuum to 800 K for 60 s by electron bombardment from the rear side. During the experiment, the temperature of the graphite crystal is held at 95 K. Nitric oxide is dosed via a differentially pumped pulsed beam ($\Delta t \sim 1$ ms) onto the surface. The low backing pressure of 20 mbar provides a nearly thermal molecular beam.[18] The pulsed beam redoses the graphite surface at 5 Hz after each desorption laser pulse, delayed by about 1 ms with respect to the detection laser pulse. Under operation of the pulsed valve, the pressure in the UHV chamber rises from 5×10^{-10} mbar to 1×10^{-9} mbar.

The free-electron laser at Hamburg (FLASH) at DESY provides XUV radiation to desorb nitric oxide from the sample in single pulses at 5 Hz repetition rate. In the present experiments, FLASH operates at photon energies of $h\nu = 38$ and 57 eV, with a temporal pulse width of about 30 fs.[19] The weakly focused $\hat{p}$-polarized FLASH beam at BL1 strikes the surface at an angle of incidence of $\vartheta_i = 67.5°$ relative to the surface normal. The sample is placed outside the focus. Due to the oblique incidence, the $200 \times 300\ \mu m^2$ ellipsoidal beam produces a 0.49 mm^2 ellipsoidal spot on the graphite. At both photon energies, average pulse energies of 24 μJ (57 eV) and between 5 and 21 μJ (38 eV) are applied, resulting in fluences of about 4 and 1 mJ/cm^2, respectively. However, due to the SASE operational principle, large pulse energy fluctuations occur.

Desorbing neutral NO molecules are detected in the gas phase at a distance of 7 mm from the surface by single color (1 + 1) resonantly enhanced multiphoton ionization (REMPI) via the $A^2\Sigma^+ \leftarrow X^2\Pi$ γ-bands around $\lambda \sim 227$ nm. The detection laser consists of a frequency tripled Nd:YAG laser (Quanta Ray, GCR-170, $\lambda = 355$ nm, $\tau = 7$ ns) pumping a commercial dye laser system (Sirah, Cobra Stretch, $\Delta\tilde{\nu} = 0.06$ cm^{-1}, $\lambda \sim 454$ nm). This output is frequency doubled in a 9 mm long BBO crystal to produce radiation tunable around $\lambda = 227$ nm. NO^+ photoions are detected by a Wiley−McLaren type time-of-flight mass spectrometer. This device is also capable of detecting ions directly desorbed by the free electron laser pulses.[15] The output of the microchannel plates is monitored on a digital oscilloscope, gated and forwarded to a computer. The NO^+ photoion signal depends linearly on the detection laser pulse energy in the range from 0.5 to 1 mJ, thus, saturating the NO γ-band transition. The rovibrational state population is then directly proportional to the detection laser pulse energy. Kinetic energy distributions for individual quantum states are measured by changing the delay between the XUV desorption laser and the detection laser. The detection laser runs in a toggle mode with twice the frequency of FLASH thereby recording signal and background separately.

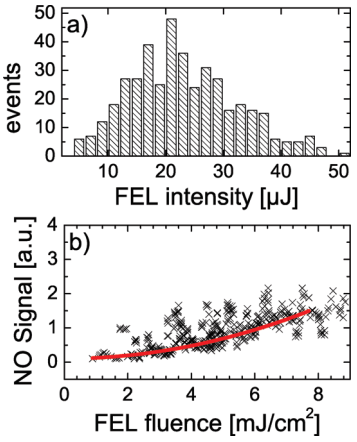

Figure 1. Histogram of the pulse energy distribution of the FLASH pulses employed. The most probable intensity is 21 μJ with a width of ±10 μJ (fwhm). (b) The NO desorption yield as a function of FEL fluence. Both figures are recorded on the bandhead of the P_{12} branch ($J'' = 8.5-12.5$) at a desorption photon energy of $h\nu = 38$ eV.

RESULTS

Fluence Dependence. A typical pulse energy distribution of the XUV FLASH pulses is shown in Figure 1a for 2000 pulses at a photon energy of $h\nu = 38$ eV. An average pulse energy of (21 ± 10) μJ is thus employed in this experiment. Figure 1b displays the dependence of the NO REMPI signal on the FEL fluence signal at the bandhead of the P_{12} branch ($v'' = 0, J'' = 8.5-12.5$), where v'', J'' denote in spectroscopic convention the vibrational and rotational quantum numbers, respectively, of electronic ground state NO molecules. A nonlinear increase of the NO REMPI signal is evident. A double logarithmic plot of the NO signal yields a slope of $n = 1.4 \pm 0.2$.

In the present study, the power dependence of the desorption yield Y is much smaller than typically observed for metal substrates where values between $Y \sim I^{3.3}$ (NO/Pd(111))[20] and $Y \sim I^{8.0}$ (CO/Cu(100))[21] have been found. However, a comparable slope with $1.3 \leq n \leq 1.6$ has been observed for the fs UV desorption of NO from NiO(100).[22] For laser desorption of NO from HOPG using nanosecond pulses of 355 nm, a linear increase of the desorption yield has recently been found.[23] The authors concluded that a single photon hot electron process induces the desorption. In most experiments concerning the photo desorption of NO from an insulator, semiconductor, or an oxidized metal, a linear dependence of the desorption yield is observed,[24,25] albeit at significantly lower peak intensities.[26]

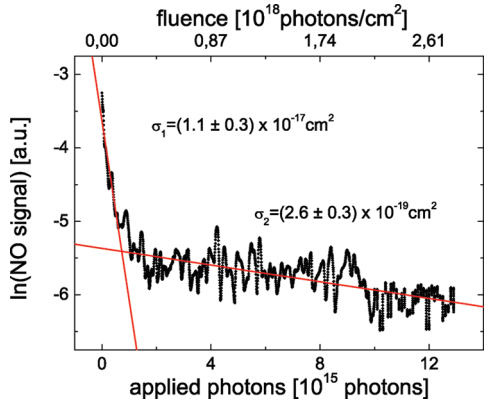

Figure 2. Desorption yield recorded on the bandhead of the P_{11} branch ($J'' = 7.5-10.5$) at a photon energy of $h\nu = 38$ eV.

For a linear dependence of the NO desorption yield, N_{des}, on the desorption laser fluence, N_{pho}/A, an effective cross section σ can be derived in the form of

$$N_{des} \propto \exp\{-\sigma N_{pho}/A\} \quad (1)$$

where N_{pho} denotes the number of photons and A is the area of the desorption laser on the surface. The desorption yield recorded at $h\nu = 38$ eV is displayed in a semilogarithmic plot in Figure 2. The double exponential decay yields for low total photon fluences a desorption cross section of $\sigma_1 = (1.1 \pm 0.4) \times 10^{-17}$ cm^2 and for high total photon fluences $\sigma_2 = (2.6 \pm 0.3) \times 10^{-19}$ cm^2 . This much lower cross section might be caused by surface diffusion of molecules from not-irradiated areas of the surface into the one already depleted by the FEL radiation at much lower total fluence. Using nanosecond pulses of 3.5 eV photon energy, Wettergren et al. observed a much lower desorption cross section of $\sigma = (2.3 \pm 0.3) \times 10^{-19}$ cm^2 for NO desorption off graphite.[23] This smaller cross section is probably caused by the low density of states around the K point making a substrate excitation difficult. The ratio of the joint density-of-states at $h\nu = 38$ eV to that at 3.5 eV is about 35. This ratio of the joint density-of-states accounts already for most of the difference in the observed desorption cross sections. An additional factor may come from the fact that in the present experiment the electronic system is excited on a time scale short compared to electronic dissipation times, while Wettergren et al. employed nanosecond pulses where dissipation occurs already during excitation.

Rovibrational Population. A wavelength scan of the detection laser across the γ-bands of NO from 227.1 to 223.7 nm yields the rovibrational state distribution of the desorbed NO molecules in the vibrational ground and the first excited state $v'' = 1$. As desorption laser FLASH produced pulses at a photon energy of hν = 57 eV with an average pulse energy of (24 ± 7) μJ. The delay between the pump and the probe laser is fixed at 24 μs, which corresponds at a probing distance of 13 mm from the surface in this case to a velocity of the detected NO molecules of 540 m/s. In Figure 3, the degeneracy corrected logarithm of the state population is plotted against the rotational energy in the form of a Boltzmann plot. The open symbols correspond to levels in the $^2\Pi_{1/2}$ fine structure state, while the filled symbols correspond to those in $^2\Pi_{3/2}$. The rotational state population is obviously nonthermal. Low rotational states with a rotational energy below 500 cm^{-1} are best fit by a rotational temperature of

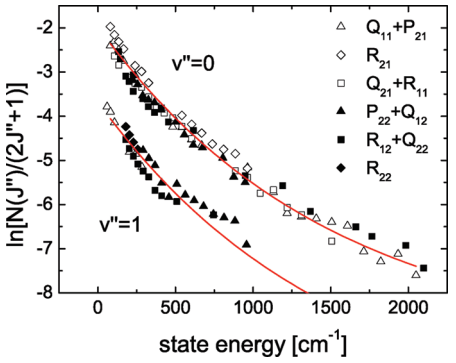

Figure 3. Rovibrational population distribution of FLASH desorbed neutral NO molecules, recorded at a pump−probe delay of 24 μs at a photon energy of $h\nu$ = 57.1 eV. The open (filled) symbols denote different rovibronic transitions originating in the $^2\Pi_{1/2}$ ($^2\Pi_{3/2}$) state. The identification of the different branches is indicated in the inset.

about $T_{rot} = 290$ K, while higher rotational states can be fitted to a temperature of $T_{rot} = 690$ K. The average rotational energy within a specific vibrational state is given by

$$\langle E_{rot}(v'')\rangle = \frac{1}{N(v'')}\sum_{J''} N_{rot}(v'',J'')E_{rot}(v'',J'') \quad (2)$$

Hereby N_{rot} denotes the population of the rotational level with the rotational energy E_{rot}. The overall rotational energy of all states of the vibrational ground state ($v'' = 0$) yields a rotational energy of $\langle E_{rot}(v''=0)\rangle = 311$ cm^{-1} corresponding to an average temperature of about $\langle E_{rot}(v''=0)\rangle/k = 448$ K. Although the average rotational energies in the two fine structure states $^2\Pi_{1/2}$ and $^2\Pi_{3/2}$ are different with $\langle E_{rot,1/2}\rangle = 189$ cm^{-1} and $\langle E_{rot,3/2}\rangle = 123$ cm^{-1}, respectively, the population in both states is in local equilibrium at the same total excitation energy, see Figure 3. The fine structure splitting in NO amounts to about 124 cm^{-1}. Averaging over the population in both states, the electronic excitation due to this fine structure excitation amounts to $\langle E_{el}\rangle = 31$ cm^{-1}. A thermal excitation of 95 K would lead to an electronic excitation of only $\langle E_{el}\rangle = 19$ cm^{-1} assuming thermal equilibrium. The observed electronic excitation then leads to an electronic temperature of $T_{el} = 172$ K. Comparing the intensities of P, Q, and R rotational branches for the same rotational state J'' allows to assess the importance of possible population differences in "e" and "f" Λ-doublet states. In the high-J'' limit (Hund's case (b)) the two Λ levels belong to different electronic symmetries. In the present case neither the "e" nor the "f" Λ-doublet states are favored in desorption. The first vibrationally excited state ($v'' = 1$) shows a similar behavior of the rotational population distribution as the vibrational ground state up to the recorded rotational state of $J'' = 21.5$. Although due to the lack of beam time the first excited vibrational state $v'' = 1$ could not be completely recorded, the most significant part was measured. The average rotational energy then amounts also to $\langle E_{rot}(v''=1)\rangle = 311$ cm^{-1}, assuming again local equilibrium between the two fine structure states as in ($v'' = 0$).

The population of a specific vibrational state can be obtained by summing the different substates involved according to

$$N_{vib}(J'') = \frac{1}{\sum_{v''}} N_{vib}(v'') \sum_{J'',\Omega''} N_{J'',\Omega''}(v'') \quad (3)$$

dx.doi.org/10.1021/jp2011793 |J. Phys. Chem. A 2011, 115, 7356–7361

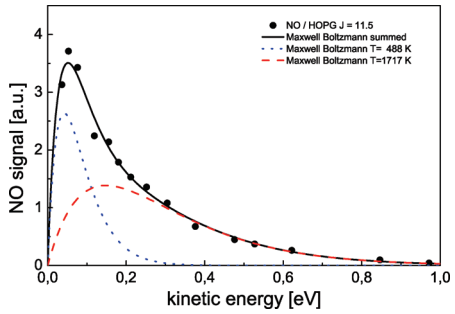

Figure 4. Kinetic energy of neutral NO molecules desorbed at $h\nu = 38$ eV in the $(Q_{22} + R_{12})$ $(J'' = 11.5)$ branch. The black dots represent the measured data, while the solid line shows the resulting fit by two Maxwellian flux distributions. The dashed and dotted lines show the two different kinetic temperatures. The Maxwellian distributions yields an average energy of $\langle E_{kin} \rangle = 170$ meV, which corresponds to a temperature of $T_{kin} = 1000$ K.

Because only a few rotational states of the $\Pi_{1/2}$ state could be analyzed in $(v'' = 1)$, the rotational population in this state has been assumed to show local equilibrium between the $^2\Pi_{1/2}$ and $^2\Pi_{3/2}$ states, as is also experimentally observed for rotational energies up to $E_{rot} \approx 300$ cm^{-1}, see Figure 3, and throughout the whole rotational states in $v'' = 0$. The population ratio of the first excited vibrational state $(v'' = 1)$ to the ground state $(v'' = 0)$ is about 0.18, resulting in a vibrational energy of $\langle E_{vib} \rangle = 136$ meV or a corresponding vibrational temperature of about $T_{vib} = 1580$ K. The vibrational temperature is thus much higher than the rotational temperature.

Kinetic Energy. A large part of the total energy in the desorbing NO molecules is released as kinetic energy. Primarily, the NO yield is measured as a function of time delay between the femtosecond XUV pulse ($h\nu = 38$ eV, (5 ± 3) μJ) and the nanosecond detection laser pulse. Both pulse durations are short compared to typical flight times in the μs-regime from the surface to the detection volume. This arrival time signal $S(t)$ is first transformed into a flight-time distribution

$$I(t) \propto S(t) \cdot \frac{L}{t} \tag{4}$$

where L denotes the flight distance and t the delay time. A Jacobi transformation then yields the desired velocity distribution

$$I(v) = \text{const} \cdot t^2 I(t) \tag{5}$$

from which the kinetic energy distribution[26]

$$I(E_{kin}) = \frac{1}{2} m_{NO} I(v^2) \tag{6}$$

is directly obtained.

Figure 4 shows this kinetic energy distribution for the $(Q_{22} + R_{12})$ $(J'' = 11.5)$ line of ground state NO. The distribution peaks at $E_{kin} = 80$ meV and slowly decreases at higher energies. NO molecules with up to 1 eV kinetic energy are observed. As an estimate of the kinetic energy release Maxwellian flux distributions are fitted to this energy distribution. Two distributions with relative yields of 35 and 65% and kinetic temperatures of $T_{kin} = 488$ K and $T_{kin} = 1717$ K, respectively, are required to fit the data, as indicated in Figure 4. For a flux distribution the average kinetic energy is given by $\langle E_{kin} \rangle = 2kT_{kin}$. Therefore, the fits yield an average energy of $\langle E_{kin} \rangle = 1370$ cm^{-1} or $T_{kin} = 1000$ K. Other rotational states at low and medium quantum number show a similar kinetic energy distribution.

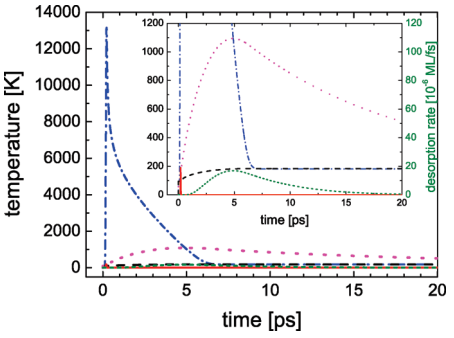

Figure 5. Temperature evolution of the electrons (blue dash-dotted line), the phonons (black dashed line), the adsorbate (magenta dotted line), and the resulting desorption flux (green short-dashed line) excited by an intense laser pulse (red solid line).

Combining these data we find that an average internal energy of $E_{int} = E_{rot} + E_{vib} + E_{el} = (38.6 + 136 + 3.9)$ meV $= 178.5$ meV is released into the desorbing NO molecules. Together with the kinetic energy of $E_{kin} = 170$ meV in total an amount of $T_{tot} = T_{int} + T_{kin} = 348.5$ meV is found in the NO molecules.

DISCUSSION

Laser-induced desorption processes are often described using the two-temperature[27] or three-temperature model[1] in which adsorbate excitation is taken into account. In the two-temperature model the electronic temperature T_{el} is coupled to the phonon temperature, T_{ph}, via

$$\frac{\partial}{\partial t} T_{el}^2 = \frac{\kappa_0}{C_{el}} \frac{\partial}{\partial z} T_{el}^2 - \frac{2T_{ph}}{C_{el}} g_\infty (T_{el} - T_{ph}) + \frac{2T_{ph}}{C_{el}} S(z,t) \tag{7}$$

$$\frac{\partial}{\partial t} T_{ph} = \frac{g_\infty}{C_{ph}(T_{ph})} (T_{el} - T_{ph}) \tag{8}$$

with C_i as specific electronic or phononic heat capacities, κ as the thermal conductivity, and g_∞ the electron−phonon coupling constant. $S(z,t)$ denotes the optical excitation. When this two-temperature model is used to describe the temperature evolution in the NO/HOPG system, a peak temperature of the electronic system of about $T_{el_{max}} \approx 13.000$ K is obtained, see Figure 5. The inset shows the temperatures of other degrees of freedom in more detail. The phononic temperature rises within 7 ps from 95 to 184 K and then slowly cools down. Within the same time the electronic system anneals to an equilibration with the phononic temperature. An exclusive coupling of a generalized adsorbate temperature to the phonon temperature of the surface would lead to a maximum desorption rate of only $d\theta/dt = 8 \times 10^{-14}$ ML/fs and an overall desorption of $\theta = 1 \times 10^{-5}$ ML per pulse. Such a phonon-mediated desorption is in the present case not responsible for the desorption process since the detected NO signal is much larger than the desorption rate calculated for this process. Also the rovibrational population measurements exclude a thermal desorption.

To gain further insight into the desorption process the coupling between the adsorbate temperature and the electronic system is considered. The equilibration time $\tau_{el-ph} = C_{ph}/g_\infty$ (see equation eq 8) implies a coupling constant of $g_\infty = 2.64 \times 10^{-17}$ W/(m^{3}K). Assuming full equilibration between the adsorbate degrees of

dx.doi.org/10.1021/jp2011793 |J. Phys. Chem. A 2011, 115, 7356–7361

freedom the translational energy of the desorbing NO can be related to the temperature of the adsorbate via $\langle E_{trans}\rangle = 2k_B T_{ads}$.[28] Therefore, the kinetic energy can be used to estimate the temperature of the adsorbate during the desorption process. For an electronically mediated process, the adsorbate temperature couples closely to the temperature of the electronic system. This results in a comparatively high temperature for a shorter period of time, while for a phonon-mediated process the adsorbate temperature is expected to be elevated much longer at a moderate temperature which, however, does not lead to the observed desorption rate.

The electronic friction model[29] couples the adsorbate temperature T_{ads} to the electronic temperature T_{el} of the substrate

$$\frac{d}{dt}T_{ads} = \eta_{el}(T_{el} - T_{ads}) \qquad (9)$$

The resulting adsorbate temperature is plotted in Figure 5 as a dotted line as a function of time after optical excitation using a coupling constant $\eta_{el} = 0.07$ ps^{-1}, as derived below. A maximum temperature of about 1100 K is reached. A yield-weighted adsorbate temperature reflects the desorption relevant temperature during the desorption process. This temperature

$$T_{ads}^{YW} = \frac{1}{\int_0^\infty R(t)dt}\int_0^\infty T_{ads}(t)R(t)dt \qquad (10)$$

can directly be compared to the kinetic energy of the desorbing molecules. From this temperature, the desorption probability is calculated to

$$P_{des} = \int R dt = E_a \int_0^\infty dt \frac{\eta}{T_{ads}} \exp[-E_a/k_B T_{ads}] \qquad (11)$$

using first order kinetics. The inset of Figure 5 shows the time dependence of the desorption rate a maximum of 17×10^{-6} ML/fs, which lasts about 6.5 ps (fwhm). Integration of $R(t)$ yields a total desorption of $P_{des} = 0.13$ ML/pulse. From the desorption cross section of $\sigma = 1.1 \times 10^{-17}$ cm^2 averaged over the first 200 pulses (see Figure 2) and an applied fluence of about 7.9×10^{14} photons/cm^2 a desorption yield of less than 0.01 ML/pulse is estimated. This yield is lower by about 1 order of magnitude compared to the model calculation. Taking, however, only the first 15 applied XUV pulses into account, the data shown in Figure 2 yield a desorption cross section of about 4.5×10^{-17} cm^2. Then, for the first pulses, one arrives at a desorption yield of 0.035 ML/pulse. Then one cautiously may conclude that not all possible attempts lead to desorption, with only every fourth trial being successful.

In the present experiment an average kinetic energy of $\langle E_{kin}\rangle = 1370$ cm^{-1} is measured, resulting in a kinetic temperature of $T_{kin} = 1000$ K. Assuming this also to be the adsorbate temperature T_{ads}, a fit of the coupling constant η_{el} to the electronic temperature yields $\eta_{el} = 0.07$ ps^{-1}. Regarding the mass dependence of the coupling constant,[29] $\eta_{el} \propto m$, this value is about a factor of 5 greater than for the H_2/Ru and D_2/Ru system where $\eta_{el} = 1/180$ and $1/360$ fs^{-1}, respectively, has been found.[30]

Desorption Mechanism. The large desorption cross sections observed in the present experiment are of the same order of magnitude as results of other experiments on nonmetallic substrates at lower photon energies. Using nanosecond pulses at $h\nu = 6.4$ eV the desorption of NO from NiO(111) occurs at a cross section of $\sigma = (6 \pm 1) \times 10^{-17}$ cm^2 decreasing to smaller values with decreasing photon energy due to a lower absorption

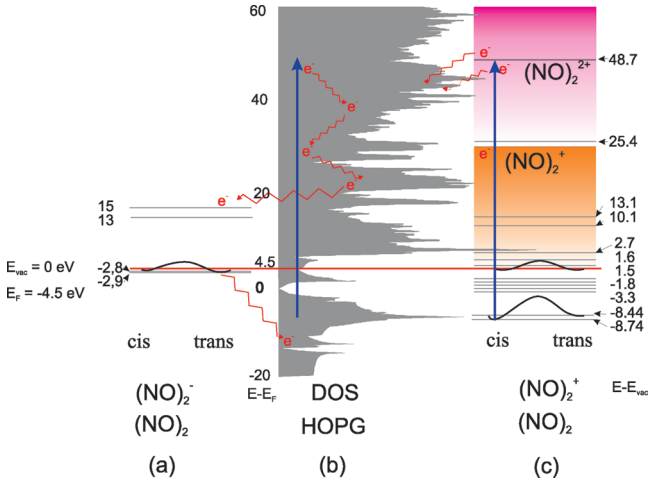

Figure 6. Electronic states of $(NO)_2$ adsorbed on graphite.[33,35]

coefficient of the NiO substrate.[31] There, a direct charge transfer reaction is induced by the exciting photons. Similarly, under the same conditions, the desorption of NO from Cr_2O_3 revealed a desorption cross section of $\sigma = (2.0 \pm 0.3) \times 10^{-17}$ cm^2.[25] When the femtosecond UV pulses are used, the desorption of NO from NiO(100) at $h\nu = 3.95$ eV yielded a desorption cross section of $\sigma = (1.9 \pm 0.3) \times 10^{-17}$ cm^2.[26] All these effective desorption cross sections are of the same order of magnitude as observed in this work for a graphite substrate, despite the fact that the applied intensities of the UV pulses employed are lower by several orders of magnitude. While for the oxide surfaces direct charge transfer excitations initiate the desorption, this is unlikely in the present case, where NO dimers are adsorbed on graphite.[32,33]

Possible excitation mechanism are shown in Figure 6. Figure 6a shows the energetics of the $(NO)_2^-$ dimer anion adsorbed on graphite. In Figure 6b the density of states (DOS) of graphite are shown. A high density of occupied states arises from the crossing region of σ and π bands at $E = -6.2$ eV. Figure 6c shows the energies for $(NO)_2^+$ cations. A direct excitation of the $(NO)_2$ adsorbate leads at photon energies of 38 eV to $(NO)_2^+$ and at 57 eV also to $(NO)_2^{2+}$ configurations. In the gas phase, the double ionization threshold occurs at $h\nu = 39.4$ eV.[34] For doubly ionized nitric oxide dimers the ionization cross section increases to about $\sigma_{max} = 1.58 \times 10^{-19}$ cm^2 at $h\nu = 49.7$ eV and then decreases to $\sigma = 1.45 \times 10^{-19}$ cm^2 at 57.1 eV. Strongly favored with ionization cross sections of $\sigma = 5.6 \times 10^{-18}$ cm^2 and 10.4×10^{-18} cm^2 at at $h\nu = 57.1$ and 38 eV, respectively, is the dissociative formation of NO^+. The dissociative ionization into atomic ions, $N^+ + O$ and $O^+ + N$, shows ionization cross sections of $\sigma = 2.3 \times 10^{-18}$ cm^2 and 1.3×10^{-18} cm^2, respectively, which unfortunately were not recorded during these runs. To summarize, these direct excitation cross sections of the adsorbate are lower than the observed desorption cross section by almost 1 order of magnitude. Although such a process can not be excluded at present, it must remain a minor contribution to the observed NO signal.

The XUV radiation is primarily absorbed in the HOPG substrate and thereby excites electrons from below the Fermi energy into highly excited states. Through electron−electron scattering or inelastic electron-defect scattering, lower energy electrons are generated. Hot electrons then may tunnel into states above the Fermi energy and thereby form a $(NO)_2^-$

complex. On graphite, the neutral $(NO)_2$ dimer is adsorbed in the *cis*-configuration, with one NO molecule lying almost flat on the surface.[32,33] For the $(NO)_2^-$ dimer anion, however, calculations[35] show that the *trans*-configuration is more attractive than a *cis*-$(NO)_2^-$ anion state by about 1000 cm^{-1}. A temporally excited anion configuration, therefore, leads not only to strongly excited vibrations as is observed on metal surfaces, but in this specific case also to a rotational excitation by inducing a transformation from a *cis*- to a *trans*-configuration. Both conclusions are supported by the observation of vibrationally excited NO ($T_{vib} \sim 1600$ K) and by a medium high rotational excitation of NO in the desorption flux.

These finding contrasts observations of UV laser-induced desorption of NO from C_{60}, where nitric oxide also adsorbs in the dimer configuration. There only a minor vibrational excitation with $T_{vib} \sim 600$ K was observed.[36] Due to the energetics a hole transfer was postulated in that case to induce the desorption. For excitation of the O_2/graphite system by XUV photons at 28 eV using synchrotron radiation a mechanism based on direct absorption in the adsorbate was found.[37] Because NO^- is isoelectronic to O_2 a similar mechanism could contribute also in that case. It seems, however, that the high photon density provided by the FEL pulses create such a high density of hot electrons in the substrate that this direct adsorbate process is obscured.

In conclusion the observations indicate that the XUV pulse induced dissociative desorption of NO from $(NO)_2$/graphite occurs via creation of a hot electron gas in graphite and a temporarily negative ion state of the adsorbate. Direct excitations of the adsorbate are at these photon energies only of minor importance.

AUTHOR INFORMATION

Corresponding Author

*E-mail: b.siemer@uni-muenster.de.

ACKNOWLEDGMENT

The authors gratefully acknowledge experimental and technical contributions by C. Thewes, S. Eppenhoff, and the mechanical workshop of the University of Münster. For helpful collaboration we want to thank the FLASH team at DESY, and acknowledge partial financial support by the Bundesministerium für Bildung und Forschung via grant No. 05 KS4PMC/8 within the research program FSP 301 "FLASH".

REFERENCES

(1) Frischkorn, C.; Wolf, M. *Chem. Rev.* **2006**, *106*, 4207.
(2) Friedrich, B.; Niedner, G.; Noll, M.; Toennies, J. P. *J. Chem. Phys.* **1987**, *87*, 1447.
(3) Chiu, Y. N.; Friedrich, B.; Maring, W.; Niedner, G.; Noll, M.; Toennies, J. P. *J. Chem. Phys.* **1988**, *88*, 6814.
(4) Farnik, M.; Toennies, J. P. *J. Chem. Phys.* **2005**, *122*, 014307.
(5) Klüner, T. *Prog. Surf. Sci.* **2010**, *85*, 278.
(6) Budde, F.; Hamza, A. V.; Ferm, P. M.; Ertl, G.; Weide, D.; Andresen, P.; Freund, H.-J. *Phys. Rev. Lett.* **1988**, *60*, 15181.
(7) Pusel, A.; Wetterauer, U.; Hess, P. *Phys. Rev. Lett.* **1998**, *81*, 645.
(8) Menzel, D.; Gomer, R. *J. Chem. Phys.* **1964**, *41*, 3311.
(9) Redhead, P. A. *Can. J. Phys.* **1964**, *42*, 886.
(10) Redlich, B.; Zacharias, H.; Meijer, G.; von Helden, G. *J. Chem. Phys.* **2006**, *124*, 044704.
(11) Tielens, A. G. G. M. *The Physics and Chemistry of the Interstellar Medium*; Cambridge University Press: Cambridge, 2006.
(12) Hornekaer, L.; Baurichter, A.; Petrunin, V.; Field, D.; Luntz, A. C. *Science* **2003**, *302*, 1943.
(13) Creighan, S. C.; Perry, J. S. A.; Price, S. D. *J. Chem. Phys.* **2006**, *124*, 114701.
(14) Ackermann, W.; et al. *Nat. Photon.* **2007**, *1*, 336.
(15) Siemer, B.; Hoger, T.; Rutkowski, M.; Treusch, R.; Zacharias, H. *J. Phys.: Condens. Matter* **2010**, *22*, 084013.
(16) Siemer, B.; Hoger, T.; Frigge, R.; Rutkowski, M.; Roling, S.; Wöstmann, M.; Düsterer, S.; Kuhlmann, M.; Plönjes, E.; Treusch, R.; Mitzner, R.; Zacharias, H. 2011, manuscript in process.
(17) Boettger, J. C. *Phys. Rev. B* **1997**, *55*, 11202.
(18) Zacharias, H.; Loy, M. M. T.; Roland, P. A.; Sudbo, A. S. *J. Chem. Phys.* **1984**, *81*, 3148.
(19) Mitzner, R.; Sorokin, A. A.; Siemer, B.; Roling, S.; Rutkowski, M.; Zacharias, H.; Neeb, M.; Noll, T.; Siewert, F.; Eberhardt, W.; Richter, M.; Juranic, P.; Tiedtke, K.; Feldhaus, J. *Phys. Rev. A* **2009**, *80*, 025402.
(20) Prybyla, J. A.; Heinz, T. F.; Misewich, J. A.; Loy, M. M. T.; Glownia, J. H. *Phys. Rev. Lett.* **1990**, *64*, 1537.
(21) Struck, L. M.; Richter, L. J.; Buntin, S. A.; Cavanagh, R. R.; Stephenson, J. C. *Phys. Rev. Lett.* **1996**, *77*, 4576.
(22) Eichhorn, G.; Richter, M.; Al-Shamery, K.; Zacharias, H. *Chem. Phys. Lett.* **1998**, *289*, 367.
(23) Wettergren, K.; Kasemo, B.; Chakarov, D. *Surf. Sci.* **2005**, *593*, 235.
(24) Kampling, M.; Al-Shamery, K.; Freund, H.-J.; Wilde, M.; Fukutani, K.; Murata, Y. *Phys. Chem. Chem. Phys.* **2002**, *4*, 2629.
(25) Wilde, M.; Seiferth, O.; Al-Shamery, K.; Freund, H.-J. *J. Chem. Phys.* **1999**, *111*, 1158.
(26) Eichhorn, G.; Richter, M.; Al-Shamery, K.; Zacharias, H. *J. Chem. Phys.* **1999**, *111*, 386.
(27) Anisimov, S. I.; Kapeliovich, B. L.; Perel'man, T. L. *Sov. Phys. JETP* **1974**, *39*, 375.
(28) Wagner, S.; Frischkorn, C.; Wolf, M.; Rutkowski, M.; Zacharias, H.; Luntz, A. C. *Phys. Rev. B* **2005**, *72*, 205404.
(29) Brandbyge, M.; Gedegard, P.; Heinz, T. F.; Misewich, J. A.; Newns, D. M. *Phys. Rev. B* **1995**, *52*, 6042.
(30) Frischkorn, C. *Surf. Sci.* **2005**, *593*, 67.
(31) Menges, M.; Baumeister, B.; Al-Shamery, K.; Freund, H.-J.; Fischer, C.; Andresen, P. *J. Chem. Phys.* **1994**, *101*, 3318.
(32) Coulomb, J. P.; Suzanne, J.; Bienfait, M.; Matecki, M.; Thomy, A.; Croset, B.; Marti, C. *J. Phys.* **1980**, *41*, 1155.
(33) Nandhakumar, I. S.; Li, Z. Y.; Palmer, R. E.; Amos, R. *Surf. Sci.* **1995**, *329*, 184.
(34) Samson, J. A. R.; Masuoka, T.; Pareek, P. N. *J. Chem. Phys.* **1985**, *83*, 5531.
(35) Urban, B.; Strobel, A.; Bondybey, V. E. *J. Chem. Phys.* **1999**, *11*, 8939.
(36) Hoger, T.; Grimmer, D.; Zacharias, H. *Appl. Phys. A: Mater. Sci. Process.* **2007**, *88*, 449.
(37) Siller, L.; Bennett, S. L.; Crabtree, H. M.; Bennett, R. A.; Wilkes, J.; Lamont, C. L. A.; MacDonald, M. A.; Palmer, R. E.; Foord, J. S. *J. Phys.: Condens. Matter* **1997**, *9*, 5815.